



# A high-performance acid-resistant polyaniline based ultrafiltration membrane: Application in the production of aluminium sulfate powder from alumina sol

Elif Gungormus, Sacide Alsoy Altinkaya\*

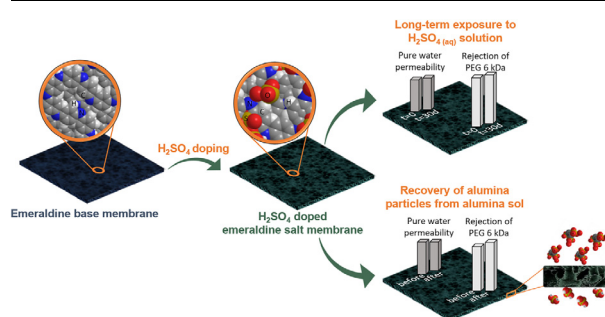
Izmir Institute of Technology, Department of Chemical Engineering, Gulbahce, Urla 35430 Izmir, Turkey



## HIGHLIGHTS

- An acid resistant polyaniline ultrafiltration membrane was developed through  $H_2SO_4$  doping.
- The performance of this membrane was tested through recovering alumina sol from  $H_2SO_4$  solution.
- Membrane was stable after 25 h acidic alumina sol filtration and 1-month storage in  $H_2SO_4$  solution.
- Membrane exhibited excellent antifouling behavior and 100% of alumina particles were recovered.
- Filtering sol can significantly reduce drying time of particles without causing agglomeration.

## GRAPHICAL ABSTRACT



## ARTICLE INFO

### Keywords:

Acid-resistant ultrafiltration membrane  
 Polyaniline  
 Antifouling  
 Alumina sol filtration  
 Aluminium salt production

## ABSTRACT

In this work, we report a new class of acid-resistant ultrafiltration membrane fabricated from polyaniline (PANI) based on its self-acid doping ability. The doped membrane was prepared by filtering the  $H_2SO_4$  solution (pH = 0.55) through the PANI membrane at 2 bar. To critically assess the acid resistance, the resulting doped membrane was stored in  $H_2SO_4$  solution (pH = 0.55) for one month. The chemical structure and separation performance of the membrane was not adversely affected by acid exposure. The membrane was also tested in realistic conditions through filtration of alumina sol synthesized in an extremely acidic  $H_2SO_4$  solution. The results have shown that 99% recovery of the aluminium sulfate particles is possible with the doped PANI membrane as a result of the hydrophilic, relatively smooth, and antifouling surface created by acid doping. The membrane filtration did not change the size and size distribution of the particles in the sol. After filtration, concentrated particles were converted into powder form in 24 h at room temperature without using a dryer. The method proposed in this study is easy and robust and can be used to develop acid-resistant UF membranes not only for concentrating the alumina sol but also for recovering valuable compounds from acid-containing feeds.

\* Corresponding author.

E-mail address: [sacidealsoy@iyte.edu.tr](mailto:sacidealsoy@iyte.edu.tr) (S. Alsoy Altinkaya).

## 1. Introduction

Most of the polymeric membranes are adversely affected by extremely acidic ( $\text{pH} \leq 2$ ) conditions. Acid-resistant membranes are needed for the recovery of nano/microparticles and various applications in metal [1,2], mining [3,4], electroplating [5], paper [6,7] industries and bio-refineries [8,9]. Among these applications, nano/microparticle recovery is attractive but highly challenging due to difficulty in preventing the permanent attachment of the particles on the membrane surface. The production of nano/microparticles in powder form is often required to lower the cost for storage and transport and for improving the stability of the particles. Previously, membranes were used for the short-term filtration of metallic nanoparticles but the filtration medium was water and the main objective was improving the efficiency of the recovery process for small scale separations [10–14]. So far the application of membranes for separation of particles from extremely acidic synthesis environment has not been reported. This is due to the lack of membranes with sufficient performance. Research efforts on developing acid-resistant membranes were mostly focused on the nanofiltration (NF) category [15–18]. Unfortunately, NF membranes are not the best choice for the recovery of nano/microparticles due to their low permeabilities. Ultrafiltration (UF) membranes are more economical alternatives than NF membranes since they can be operated at lower pressures. In addition to the energy cost, the overall cost of recovering particles with membranes is also determined by the cost of the membrane polymer. Semicrystalline polymers such as polytetrafluoroethylene (PTFE), polyethylene (PE), polyvinylidene fluoride (PVDF), poly(ether ether ketone) (PEEK), ethylene chlorotrifluoroethylene (ECTFE), chlorinated polyvinyl chloride (CPVC), and perfluoroalkoxy alkane (PFA) are known to be acid-resistant [19–25]. However, the usage of these polymers is limited to small scale membrane production due to high raw material costs. Also, their extreme hydrophobicities result in low-flux membranes with a high fouling tendency. The review of current studies then clearly indicated that efficient and cost-effective acid-resistant UF membranes are needed.

This study aims to fill the gap in the literature regarding the development of acid-resistant UF membranes. Polyaniline (PANI) was chosen as a membrane polymer since it can be synthesized using low-cost monomers and easily doped by protonic acids [26] to impart acid resistance. Besides, it has high thermal and chemical stability and a hydrophilic structure [27]. The performance of this membrane was tested through filtration of aluminium sulfate particles (alumina sol) synthesized in an extremely acidic  $\text{H}_2\text{SO}_4$  solution. The separation of particles from the acid solution is required for both controlling the size, size distribution of the particles and for obtaining powder. Traditionally, aluminium sulfate powder is produced by freeze-drying, spray-drying, and conventional drying of alumina sol in an oven at different temperatures and pressures [28,29]. However, the production method solely utilizing drying has serious disadvantages. First, drying times are typically long due to low solid content in the sol. This causes both very high energy usage and a reduction in the service life of the dryers due to corrosion. Second, Van der Waals forces and Brownian motion can cause agglomeration in a conventional drying process [30–32]. This is certainly undesirable since the powder with a narrow size distribution is required for applications. Third, a significant amount of acid loss occurs during drying which is not only an economic loss but has also a negative impact on the environment. Membrane filtration prior to drying can help to minimize these disadvantages. However, to scale up the use of membranes for concentrating the sol from the acid solution, they should have long-term acid resistance and antifouling properties. This study focused on both of these challenges. In this context, the acid resistance of the developed membrane was evaluated by determining the change in chemical structure, surface morphology, elemental compositions and pore size of the membrane upon long-term exposure to  $\text{H}_2\text{SO}_4$  acid solution. The fouling tendency of the membrane was

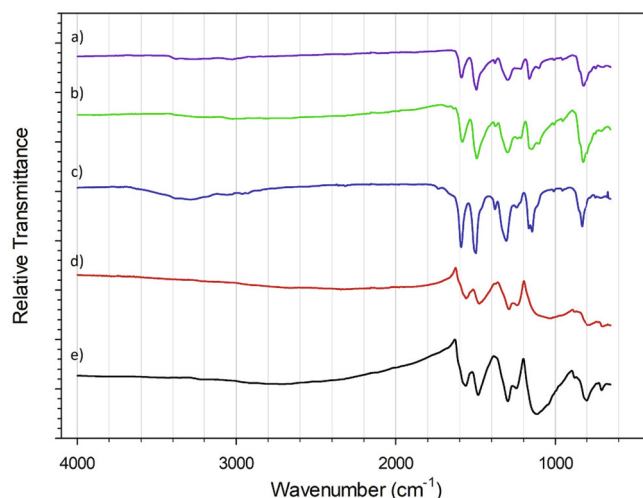


Fig. 1. ATR-FTIR spectra of a) synthesized and b) commercial EB in the form of polymer, c) EB membrane, d)  $\text{H}_2\text{SO}_4$  doped ES membrane and e)  $\text{H}_2\text{SO}_4$  doped ES membrane after 30 days of  $\text{H}_2\text{SO}_4$  exposure under static conditions.

evaluated through following flux change during alumina sol filtration and comparing the pure water fluxes of the clean and backwashed membranes after sol filtration. In addition, the impact of membrane filtration on the chemical and physical properties of the aluminium sulfate powder was investigated. In light of the literature, the novelty of this study lies in three points. First, it proposes a new acid-resistant PANI based UF membrane which can easily be obtained through a simple acid doping process. Second, it is shown for the first time that acid-doped PANI membrane can be used for the recovery of aluminium sulfate particles from extremely acidic synthesis environment without the permanent attachment of particles on the surface. Third, this study is the first which demonstrates the production of aluminium sulfate powder from the sol through membrane filtration without using a dryer.

## 2. Materials and methods

### 2.1. Materials

Aniline (Sigma-Aldrich, ACS reagent,  $\geq 99.50\%$  purity), ammonium persulfate ( $(\text{NH}_4)_2\text{S}_2\text{O}_8$ , Sigma-Aldrich, ACS reagent,  $\geq 98\%$  purity), HCl fuming 37% (Merck), 25% ammonia solution ( $\text{NH}_4\text{OH}$ , Merck), and methanol (Sigma-Aldrich, ACS reagent,  $\geq 99.80\%$  purity) were utilized to synthesize PANI. Commercial EB (average Mw  $\sim 100,000$ ) was supplied from Sigma Aldrich. Triethylamine (Riedel-de Haën) and N-methyl-2-pyrrolidone (NMP, Merck, anhydrous, greater than 99.5%) were used to prepare casting solution. PEG 1000, 4000, 6000, 10000, and 20000 Da provided by Sigma Aldrich were used to determine MWCO.  $\text{H}_2\text{SO}_4$  ( $\geq 98\%$  purity) used in membrane doping process and alumina sol synthesis and aluminum isopropoxide ( $\geq 98\%$  purity) used in the preparation of alumina sol were all purchased from Sigma-Aldrich.

### 2.2. Synthesis of the emeraldine base (EB) form of PANI

EB is the most extensively studied form of PANI due to having higher environmental stability compared to other forms. PANI was synthesized through chemical oxidative polymerization of aniline in a medium of HCl aqueous solution by using  $(\text{NH}_4)_2\text{S}_2\text{O}_8$  as an oxidizing agent. Aniline and  $(\text{NH}_4)_2\text{S}_2\text{O}_8$  were separately dissolved in 1 M HCl solution and their concentrations were adjusted to 10% (v/v) and 5% (w/v), respectively. The prepared solutions were cooled to 0 °C, then the oxidant solution was added dropwise to aniline solution under

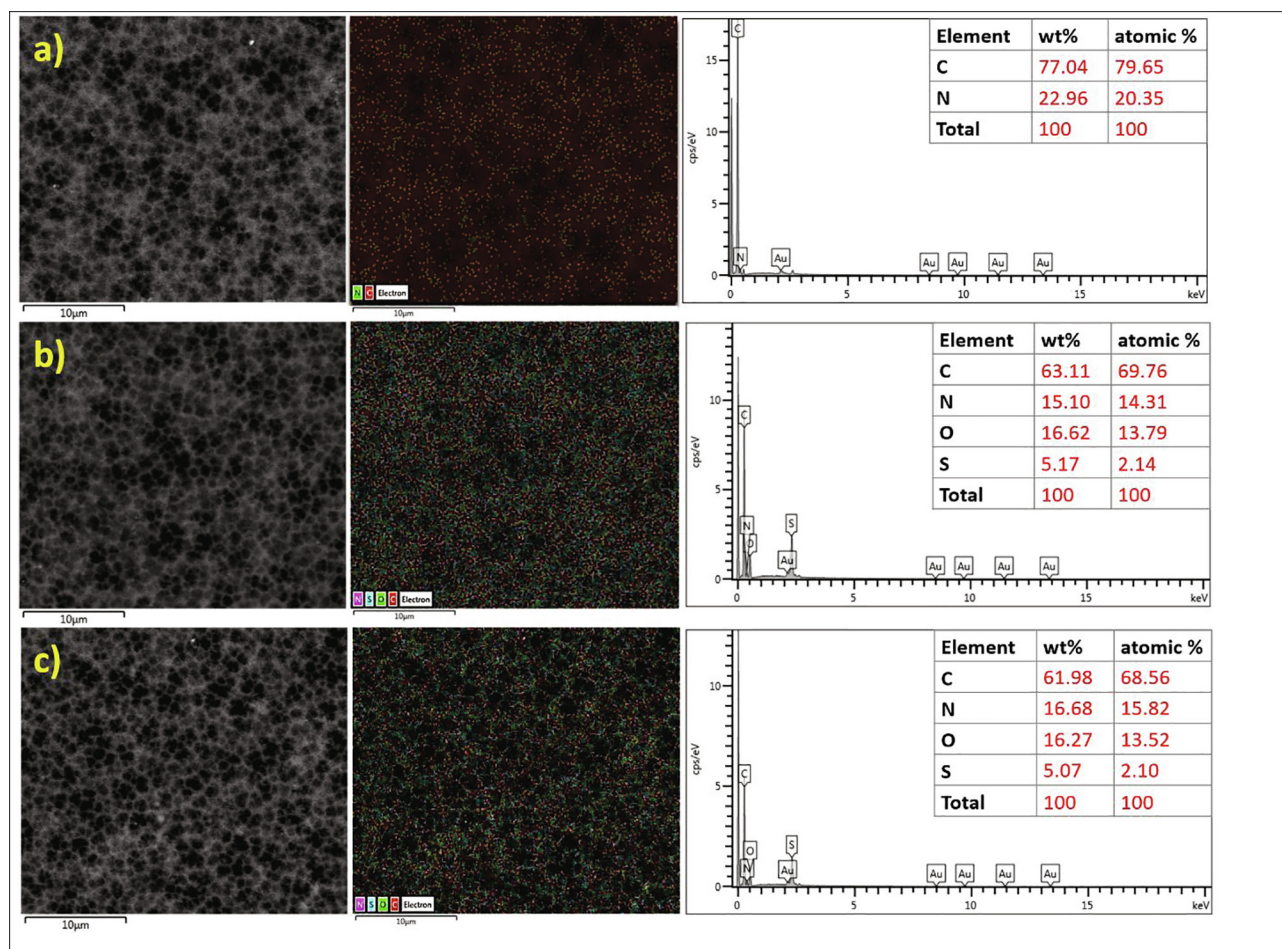


Fig. 2. SEM-EDX elemental analysis and mapping of a) EB membrane, b) H<sub>2</sub>SO<sub>4</sub> doped ES membrane, and c) H<sub>2</sub>SO<sub>4</sub> doped ES membrane after 30 days of H<sub>2</sub>SO<sub>4</sub> exposure under static conditions.

constant stirring. The polymerization reaction was carried out first at 0 °C for 4 h to limit secondary reactions and then at 25 °C for 20 h. At the end of the reaction, the color of the mixture turned from transparent to dark green, and a solid deposit was formed. The deposit was filtered and rinsed first with 1 M HCl solution and next with deionized water (DI). The washing process was continued until the pH of the washing solution became 7. The filtered emeraldine hydrochloride precipitate was treated with 1 M NH<sub>4</sub>OH solution for 3 h to obtain EB, rinsed with DI water until the pH of DI water was reached and finally washed with water: methanol mixture and then filtered. The dark blue EB powder was dried for 48 h under vacuum. The general procedure for EB synthesis was adapted from the studies conducted by Gomes and Oliveira [33] and Ibrahim [34].

### 2.3. Preparation of the EB and H<sub>2</sub>SO<sub>4</sub> doped emeraldine salt (ES) membranes

The synthesized EB was dried at 70 °C for 4 h to remove moisture. NMP was mixed with gel inhibitor trimethylamine, next EB was gradually added and the mixture was stirred continuously for 1 h at 300 rpm (T = 25 °C). The concentrations of EB, trimethylamine, and NMP in the solution were adjusted to 15 wt%, 1.50 wt%, and 83.50 wt %, respectively. In order to eliminate air bubbles, the solution was held without stirring for 1 h, and then cast on a polyester nonwoven fabric (Type TH, Hirose Paper Mfg. Co. Ltd.) with the help of an automated film applicator (Sheen Instrument Ltd., model number: 1133N) and finally immediately immersed into water bath at 20 °C. The initial thickness of the cast membrane was adjusted as 200 μm. This

membrane was first compacted at 2 bar until reaching steady-state condition, then, doped by filtering 0.27 M H<sub>2</sub>SO<sub>4</sub> aqueous solution (pH = 0.55) at 2 bar for 3 h. These prepared un-doped and acid doped membranes will be referred to as the EB and H<sub>2</sub>SO<sub>4</sub> doped ES membranes, respectively. The doping time of 3 h was enough to achieve a constant flux.

### 2.4. Performance tests of the EB and H<sub>2</sub>SO<sub>4</sub> doped ES membranes

A dead-end cell filtration system with a cell volume of 10 ml and an effective surface area (A) of 4.10 cm<sup>2</sup> (Millipore, Amicon Stirred Cell 8010) was used in performance tests of the membranes. The prepared membranes were compacted until reaching steady state conditions, then the volume of permeated water (ΔV) was recorded for every one minute (Δt) at a constant transmembrane pressure difference (ΔP) of 1 bar. Pure water permeability (PWP, Lm<sup>-2</sup>h<sup>-1</sup>bar<sup>-1</sup>) of the membranes was calculated by using Eq. (1).

$$PWP = \frac{\Delta V}{A \times \Delta t \times \Delta P} \quad (1)$$

The rejection properties of the membranes were tested with aqueous solutions of PEG (1 g/L) with a molecular weight of 1000, 4000, 6000, 10000, and 20000 Da, separately. The PEG solutions were filtered at 1 bar under a constant stirring rate of 200 rpm, and the concentrations of feed (C<sub>F</sub>), retentate (C<sub>R</sub>), and permeate (C<sub>P</sub>) solutions were detected by using Rudolph-J357 Automatic Refractometer. The rejection levels (R, %) were calculated from

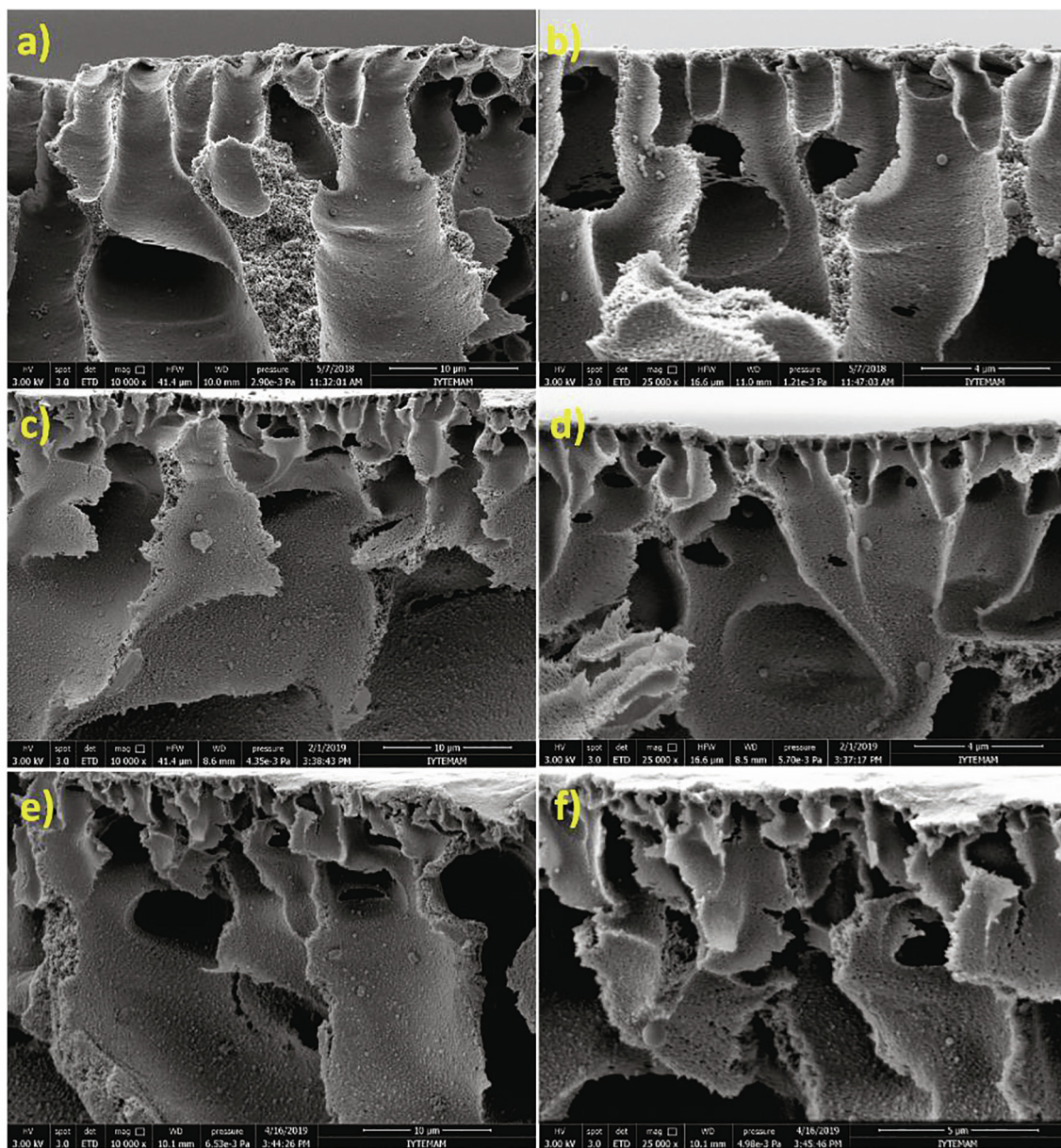


**Fig. 3.** Cross-section SEM images of a-b) EB membrane, c-d)  $H_2SO_4$  doped ES membrane and e-f)  $H_2SO_4$  doped ES membrane after 30 days of  $H_2SO_4$  exposure under static conditions with a magnification of  $\times 10000$  and  $\times 25000$ , respectively.

$$R(\%) = \left( 1 - \frac{C_P}{0.5 \times (C_F + C_R)} \right) \times 100 \quad (2)$$

The feed concentration in the module ( $C_F$ ) changes with time due to the decrease in volume and increase in amount rejected by the membrane. In order to take the change in concentration on the feed side into account, an arithmetic average of the concentrations measured at the beginning ( $C_F$ ) and at the end of the rejection experiment ( $C_R$ ) were used [35].

### 2.5. Characterization of the EB and $H_2SO_4$ doped ES membranes

Pore size of the membrane was predicted from the rejection data collected using PEG solutions. For uncharged solutes, at high pore Peclet number, the rejection of a solute is given by the following equations by assuming that pores in the membrane are cylindrical [36,37]:

$$R_{lim} = 1 - \Phi K_{i,c} \quad (3)$$

$$\Phi = (1 - \lambda^2) \quad (4)$$

$$K_{i,c} = (2 - \Phi)(1 + 0.054\lambda - 0.988\lambda^2 + 0.441\lambda^3) \quad (5)$$

$$\lambda = \frac{r_s}{r_p} \quad (6)$$

where  $\phi$ ,  $K_{i,c}$ ,  $r_s$ , and  $r_p$  are the steric partition coefficient, the hindrance factor for convection, the solute and pore radii (in nm), respectively. The radius of PEG was predicted from Eq. (7) which was derived from Stokes-Einstein law by assuming PEG as a spherical particle.

$$r_s = 0.045 \times MW^{0.44} \quad (7)$$

where the unit of molecular weight ( $MW$ ) is Da.

The chemical structure of the dried membranes was determined with Attenuated Total Reflectance Fourier Transformed Infrared Spectrometer (ATR-FTIR, Perkin Elmer) at ambient temperature over a scanning range of  $650\text{--}4000\text{ cm}^{-1}$  with a resolution of  $4.00\text{ cm}^{-1}$ . The surface and bulk morphology of the membranes was observed with the scanning electron microscope (SEM) (FEI Quanta 250 FEG) and

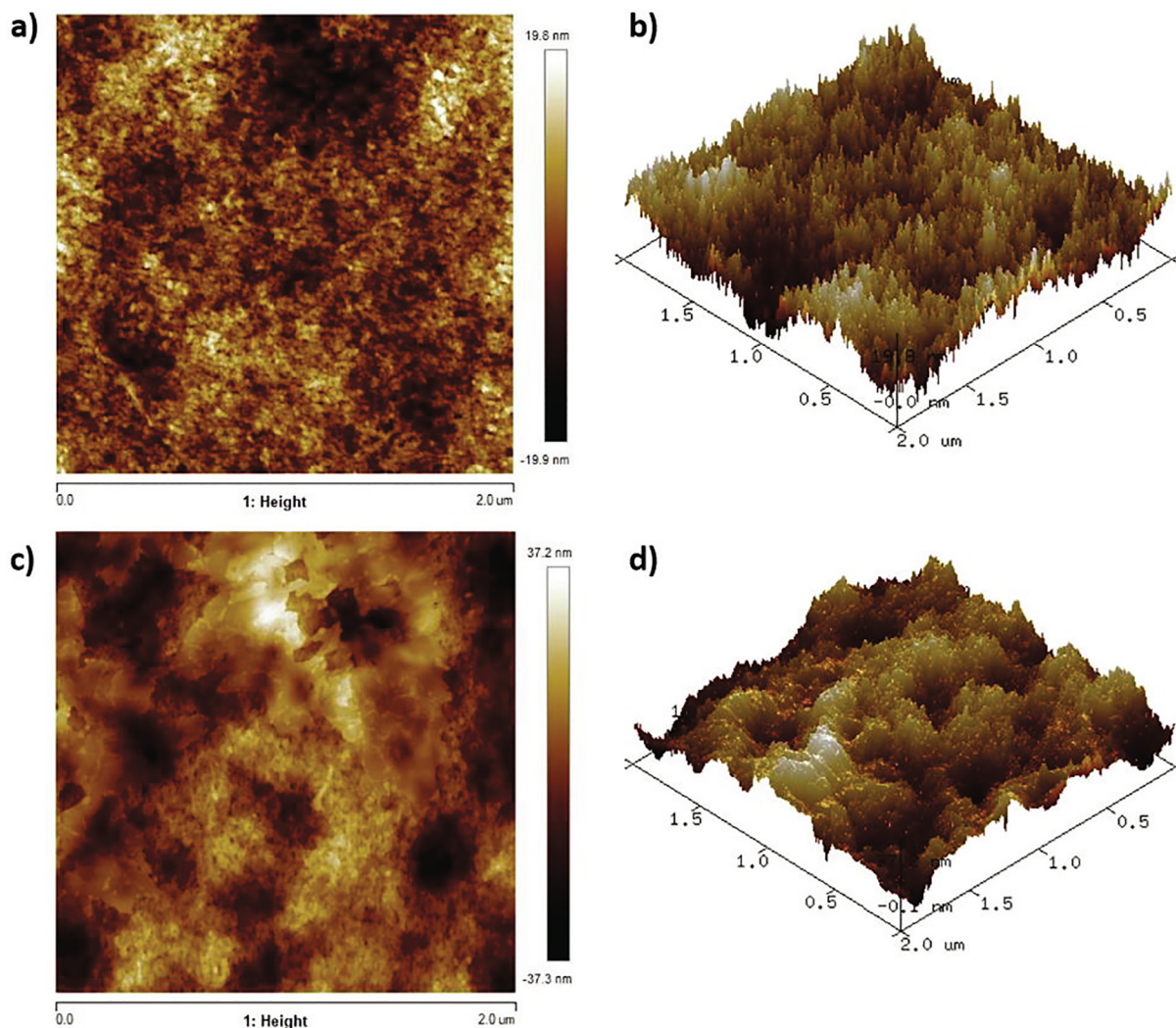


Fig. 4. AFM images of a-b) EB membrane and c-d) H<sub>2</sub>SO<sub>4</sub> doped ES membrane.

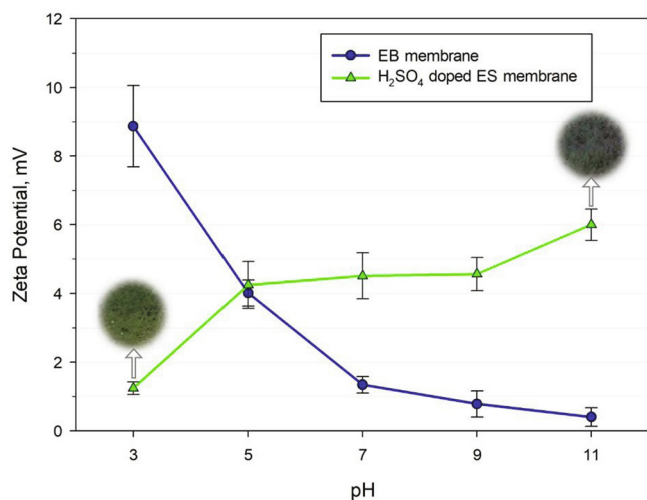


Fig. 5. Zeta potential of EB and H<sub>2</sub>SO<sub>4</sub> doped ES membranes as a function of pH.

elemental compositions on the surface were determined with energy dispersive X-ray analysis (EDX). The membranes were fractured in liquid nitrogen and sputter-coated with gold to obtain a clear cross-

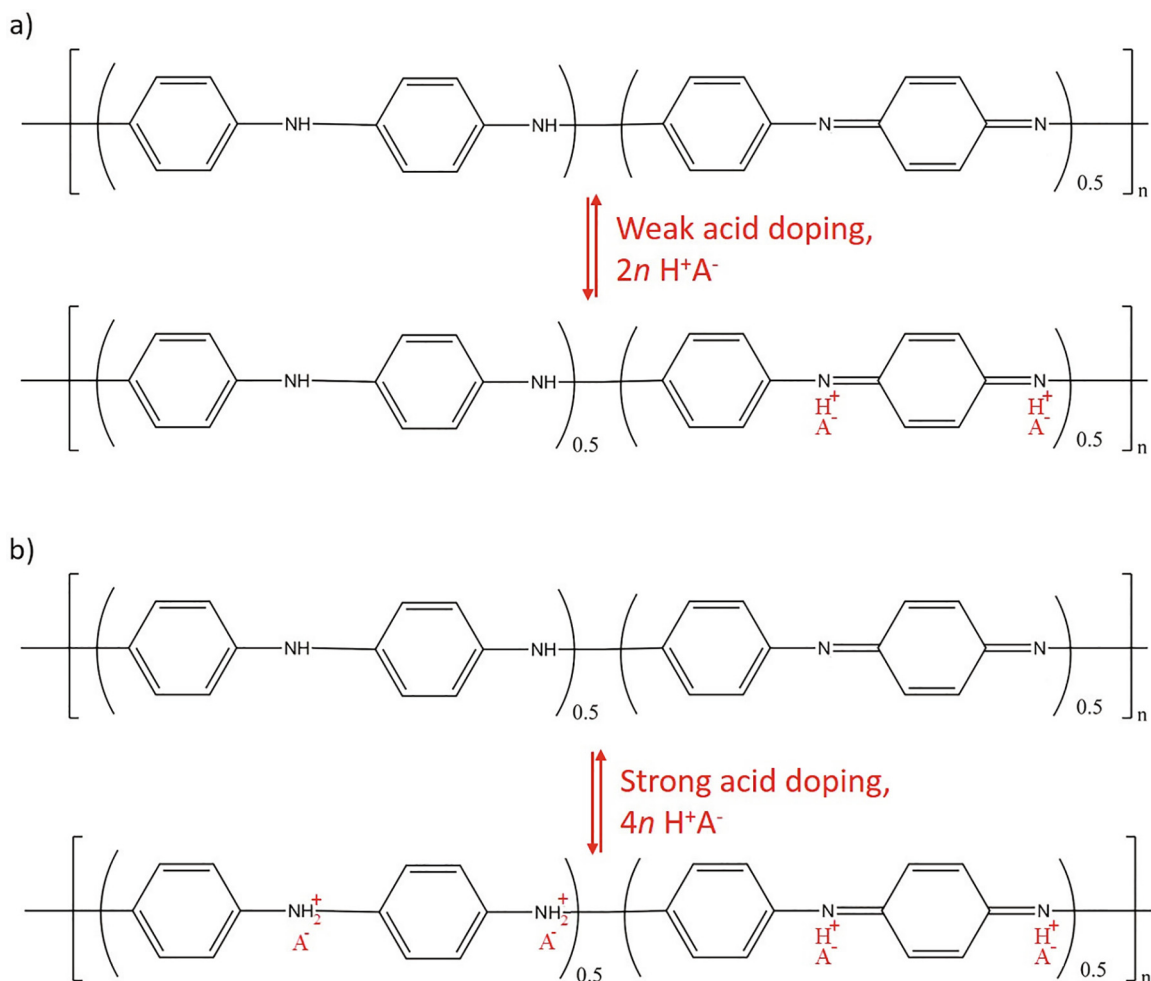
section. The surface roughness of the membranes was determined with atomic force microscopy (AFM, MMSPM Nanoscope 8 Bruker) by taking topographic images of 2 μm × 2 μm sized dried membrane surfaces at a rate of 1 Hz. Zeta potential values of the membranes in 10 mM NaCl solution were measured by NanoPlus Micromeritics Instrument. NaCl solution was adjusted to five different pH level in the range of 3–11, by using HCl and NaOH for acidic and basic pH, respectively. Membrane hydrophilicity was characterized by measuring dynamic contact angles of the dried membrane (Attension Optical tensiometer) with 5 μl of the deionized water droplet.

#### 2.6. Acid resistance of the H<sub>2</sub>SO<sub>4</sub> doped ES membrane

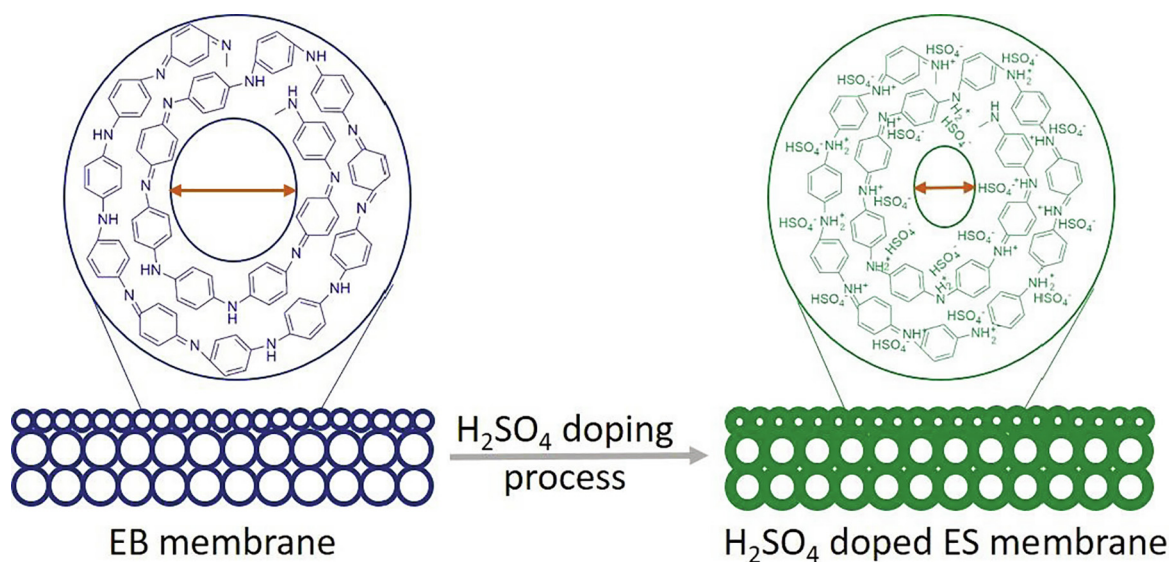
The dense surface of the H<sub>2</sub>SO<sub>4</sub> doped ES membrane was exposed to a 0.27 M H<sub>2</sub>SO<sub>4</sub> solution for one month at room temperature. The PWP and PEG 6000 rejection of the membrane were measured before and after acid exposure (exposure to acid solution). In addition, the chemical structure, surface morphology, and elemental compositions of the fresh and acid-exposed membranes were investigated by using ATR-FTIR, SEM, and EDX analyses.

#### 2.7. Preparation of alumina sol and determination of its particle size distribution

Alumina sol was synthesized using the procedure given in the study



**Scheme 1.** Rearrangement reaction mechanism between the EB and ES polymers through a) weak protonic acid b) strong protonic acid doping and dedoping in alkaline medium.  $\text{A}^-$  is an anion of the protonic acid.



**Scheme 2.** Proposed mechanism for pore size reduction in the bulk of the membrane due to  $\text{H}_2\text{SO}_4$  doping.

of Yoldas [38]. Deionized water at  $85^\circ\text{C}$  and aluminum isopropoxide was mixed and stirred for 1 h at  $85^\circ\text{C}$ .  $\text{H}_2\text{SO}_4$  was added to the mixture (aluminum isopropoxide:  $\text{H}_2\text{SO}_4$ : water 1 g: 0.65 ml: 10.25 ml), stirred again for 1 h at the same temperature and finally, a clear sol was

formed. The prepared alumina sol was kept at room temperature for 1 day before further use. The particle size distribution of the sol was determined using DI water as a solvent (NanoPlus Micromeritics).

**Table 1**  
H<sub>2</sub>SO<sub>4</sub> stability of different polymeric membranes.

Membrane	Membrane Chemistry	Storage time and temperature	Molarity of H <sub>2</sub> SO <sub>4</sub> solution	Permeability increment (Lm <sup>-2</sup> hr <sup>-1</sup> bar <sup>-1</sup> )	Rejection decline	Reference
BPT-NF-1-006	Melamine polyamine with polyether sulphone support membrane	30 days, 80 °C 2 months, 80 °C	2.04	1.7–3.9 to 23.2–27.3 1.7–3.9 to 60.8–65	83–91.5% to 28.5–30.4% for sucrose in water 75–88% to 14.9–19.8% for glucose in water 83–91.5% to 8.6–12.9% for sucrose in water	Platt et al. [51]
		30 days, 20 °C 4 months, 20 °C		1.7–3.9 to 3–3.2 1.7–3.9 to 3–3.1	75–88% to 8–8.9% for glucose in water 83–91.5% to 81.5–82% for sucrose in water 75–88% to 77.7–82% for glucose in water 83–91.5% to 85.2–86 for sucrose in water	
		30 days, 20 °C 3 months, 20 °C	1.22	2.22 to 2.3 2.22 to 4.3	75–88% to 82–82.8% for glucose in water 96% to 95% for sucrose in water 92% to 90% for glucose in water 96% to 90% for sucrose in water	
BPT-NF-2-015	Melamine polyamine with polyether sulphone support membrane	30 days, 80 °C 2 months, 80 °C 30 days, 20 °C 4 months, 20 °C	2.04	1.8–4.9 to 41.3–54.6 1.8–4.9 to 85.8–129 1.8–4.9 to 4.7–4.8 1.8–4.9 to 5.3–5.4	88–97% to 8.1–16.2% for sucrose in water 78–93% to 6.2–9.8% for glucose in water 88–97% to 6.1–9.9% for sucrose in water 78–93% to 1.6–5.9% for glucose in water 88–97% to 90.8–92.9% for sucrose in water 78–93% to 82.7–87.5% for glucose in water 88–97% to 82.2–83% for sucrose in water 78–93% to 70.2% for glucose in water	Liu et al. [15]
PIP-NTSC	Piperazine-naphthalene-1,3,6-trisulfonylchloride composite	2 months, 25 °C	2.04	5.72 to 6.5	~90% to 86% for Na <sub>2</sub> SO <sub>4</sub> in water	Liu et al. [15]
PIP-PA	Piperazine-polyamide	24 hr, 55 °C	1.02	~1.44 to ~ <sup>ab</sup> ~1.18 to ~ <sup>ab</sup>	~72% to ~ <sup>b</sup> for MgSO <sub>4</sub> in water ~96% to ~ <sup>b</sup> for MgSO <sub>4</sub> in water	Hoseinpour et al. [18]
MPD-PA	M-phenylenediamine- polyamide			~2.24 to 6.6 <sup>b</sup>	~68% to 32 for MgSO <sub>4</sub> in water	
MPD-PASA	Piperazine-poly(amide-sulfonamide)			~1.82 to 9.4 <sup>b</sup>	~70% to 20 for MgSO <sub>4</sub> in water	
PIP-PSA	Piperazine-Polysulfonamide			~2.6 to 2.8 <sup>a</sup>	~46% to 44 for MgSO <sub>4</sub> in water	
MPD-PSA	M-phenylenediamine- Polysulfonamide			~1.56 to 1.8 <sup>b</sup>	~32% to 25 for MgSO <sub>4</sub> in water	Ricci et al. [50]
MPP-34	Proprietary composite	4 weeks, 20 °C	0.15	3.1 to 13.3	97% to 70% for MgSO <sub>4</sub> in water 97% to 84% for CoSO <sub>4</sub> in water 98% to 71% for NiSO <sub>4</sub> in water	
MPP-34	Proprietary composite	8 weeks, 20 °C			97% to 19% for MgSO <sub>4</sub> in water 97% to 19% for CoSO <sub>4</sub> in water 98% to 33% for NiSO <sub>4</sub> in water 97% to ~92% for MgSO <sub>4</sub> in water	Zeng et al. [16]
TPT-TMC/PSF	1,3,5-(tris-piperazine)-triazine- trimesoyl Chloride/Polysulfone	30 days, 25 ± 1 °C	0.05	~8 to 12	95% to 62% for MgSO <sub>4</sub> in water	
PIP-TMC/PSF	Piperazine- trimesoyl Chloride/Polysulfone			7.11 to 15.16		
PES-PSA5	Polyethersulphone- polysulfonamide	24 h, 90 °C	2.04	3.03 to 5.49 1.49 to 3.21 9.23 to 23.55	99.81% to 95.92% for Na <sub>2</sub> SO <sub>4</sub> in water 98.31% to 95.97% for Na <sub>2</sub> SO <sub>4</sub> in water 99.16% to 28.49% for Na <sub>2</sub> SO <sub>4</sub> in water	He et al. [17]
Control IP	2,4,6-tris(chlorosulfonyl)phenol- piperazine					
TMC-PIP	Trimesoyl Chloride- piperazine					
NF270	Polyamide	24 h, 20 °C	12.5	11.64 to 50.04 8.2 ± 1.2 to 10.14	99.42% to 4.36% for Na <sub>2</sub> SO <sub>4</sub> in water	Lohokare et al. [54]
M1	Poly(2,5-benzimidazole)-polypropylene			15.1 ± 1.5 to 20.55		
M6				6.8 to 7.6		
NF6	Polysulfonamide	30 days, 21 °C	2.04	~0.5 to 0.48	92% to 88% for MgCl <sub>2</sub> in water	Wang et al. [52]
PSA-PSF	Polysulfonamide-polysulfone	24 h, 25 ± 5 °C	0.82	~2.5 to 4.2	~86% to 87 for Na <sub>2</sub> SO <sub>4</sub> in water	Zhu et al. [53]
PSA/SPEEK-PSF	Polysulfonamide/ sulfonated poly(ether ether ketone)-polysulfone				~89% to 88 for Na <sub>2</sub> SO <sub>4</sub> in water	
SPEEK-PSF	sulfonated poly(ether ether ketone)-polysulfone			~3.2 to 7	~88% to 75 for Na <sub>2</sub> SO <sub>4</sub> in water	

(continued on next page)

Table 1 (continued)

Membrane	Membrane Chemistry	Storage time and temperature	Molarity of H <sub>2</sub> SO <sub>4</sub> solution	Permeability increment (Lm <sup>-2</sup> hr <sup>-1</sup> bar <sup>-1</sup> )	Rejection decline	Reference
H <sub>2</sub> SO <sub>4</sub> doped ES membrane	Emeraldine salt	30 days, 20 ± 1 °C	0.27	25.47 ± 0.06 to 25.59 ± 0.07	87.78 ± 0.38% to 87.92 ± 0.29% for PEG 6000 in water	This study

<sup>a</sup> Permeability of salt aqueous solution with the unit of kgm<sup>-2</sup>hr<sup>-1</sup>bar<sup>-1</sup>.

<sup>b</sup> Membrane completely degraded in H<sub>2</sub>SO<sub>4</sub> aqueous solution.

## 2.8. Alumina sol filtration performance of the H<sub>2</sub>SO<sub>4</sub> doped ES membrane

The alumina sol was filtered through H<sub>2</sub>SO<sub>4</sub> doped ES membrane at 1 bar under a constant stirring rate of 200 rpm until the volume of the sol was reduced to 20% of the feed solution. Experiments started with the measurement of PWP of the membrane. After filtering 40 ml of the sol, the membrane ( $A = 4.10 \text{ cm}^2$ ) was backwashed with water for 30 min and the PWP was re-measured to evaluate the extent of flux recovery. This cycle was repeated for 4 times and 80% volume reduction of the sol was achieved in 5 cycles. The recovery of the alumina sol ( $Rec.$ ) was calculated from Eq.8 by measuring the mass of dried feed ( $W_F$ ), retentate ( $W_R$ ), permeate ( $W_P$ ) and backwashing ( $W_B$ ) solutions.

$$Rec(\%) = \left( \frac{W_R + W_B}{W_F} \right) \times 100 \quad (8)$$

Flux recovery ratios ( $FRR$ ), reversible fouling ( $R_r$ ) and irreversible fouling ( $R_{ir}$ ) resistances were calculated by using the following equations.

$$FRR(\%) = \frac{J_R}{J_W} \times 100 \quad (9)$$

$$R_r(\%) = \frac{J_R - J_P}{J_W} \times 100 \quad (10)$$

$$R_{ir}(\%) = \frac{J_W - J_R}{J_W} \times 100 \quad (11)$$

where  $J_W$  and  $J_R$  are the pure water fluxes of the clean and backwashed membranes after sol filtration, respectively, while  $J_P$  is the flux of alumina sol.

## 2.9. Preparation and characterization of powder obtained with and without filtration of alumina sol

After filtering 80% of alumina sol, concentrated particles were converted into powder form simply by drying at room temperature without using a dryer. For a comparison, alumina sol was also dried in a freeze dryer and in an oven at 100 °C without applying filtration. Drying continued until reaching a constant weight of powder. The shapes of powders were observed by SEM (FEI Quanta 250 FEG), while the particle size distribution was determined with NanoPlus Micromeritics Instrument by dispersing the powder in deionized water. Each measurement was made in triplicate to ensure repeatability. The crystal structure of the powders was characterized by X-ray diffractometer (XRD, Philips X'pert Pro Diffractometer – operated at 40 kV, 45 mA) with Ni-filtered CuK $\alpha$  radiation ( $\lambda = 0.15406 \text{ nm}$ ) in the range of 5–80° 2 $\theta$  angle. The crystalline phases in powders were identified using Powder Diffraction File of International Centre for Diffraction Data [39].

## 3. Results and discussion

### 3.1. Characterization of the EB and H<sub>2</sub>SO<sub>4</sub> doped ES membranes

Fig. 1 shows that the IR spectra of the synthesized and commercial EB polymers are equivalent which proved the success of polymer synthesis. For EB in the form of polymer and membrane, the typical peaks located at 1600 and 1500 cm<sup>-1</sup> are respectively assigned to the stretching vibration of nitrogen quinoid and benzenoid [40], as shown in Fig. 1.a-c. The band at 1300 cm<sup>-1</sup> also originated from the C–N stretch of a secondary amine group. The aromatic C–H in-plane bending modes were observed in the region of 1010–1170 cm<sup>-1</sup> [41–43]. H<sub>2</sub>SO<sub>4</sub> doping caused shifting in the peaks of the quinoid, benzenoid, and the secondary amine to 1563, 1480, and 1291 cm<sup>-1</sup>, respectively (Fig. 1.d). This indicates the quinone and benzene ring-stretching deformations, due to the protonation of the nitrogen of amine and imine groups in the

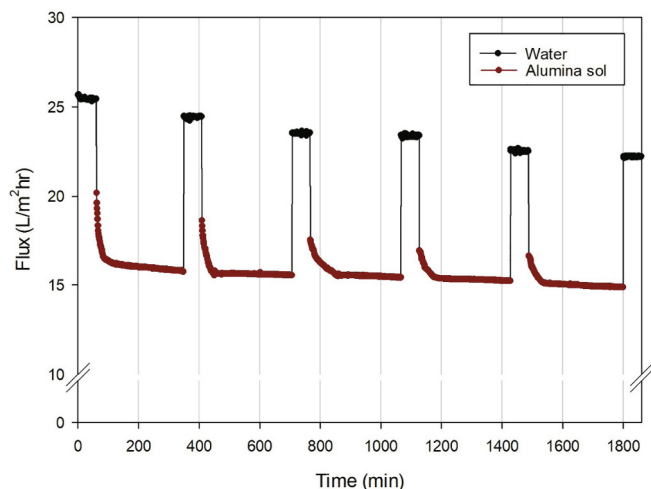


**Fig. 6.** Performance of H<sub>2</sub>SO<sub>4</sub> doped ES membrane during 5-cycle alumina sol filtration.

EB chain [42,44]. The peaks at 1200, 1147, and 1054 cm<sup>-1</sup> are assigned to C–N<sup>+</sup> stretching vibration, –NH<sup>+</sup>= stretching vibration, and S=O bonds which are formed during protonation of EB with H<sub>2</sub>SO<sub>4</sub>. The aromatic C–H in-plane vibration and out-of-plane vibration are also observed in the range of 1010–1170 cm<sup>-1</sup> and 807–881 cm<sup>-1</sup>, respectively. These peaks overlap a broad absorption extending from 850 to 1200 cm<sup>-1</sup>. The appearance of the specific peaks exhibiting chemical bonds of EB and H<sub>2</sub>SO<sub>4</sub> doped ES membranes approves the

successful EB membrane synthesis and effective acid doping process to the EB membrane.

The elemental composition of the membrane surfaces obtained from EDX analysis is shown in Fig. 2. Compared to the pristine EB membrane, the presence of sulfur and oxygen in the modified membrane also proved successful H<sub>2</sub>SO<sub>4</sub> doping. SEM-EDX mapping images demonstrated a homogeneous distribution of sulfur and oxygen on the surface. Cross-section SEM images shown in Fig. 3 illustrate that both doped and un-doped membranes have typical finger-like pores in the sublayer along with a thin dense active layer on top of the porous support layer. Acid doping did not significantly change the bulk morphology of the membrane, on the other hand, the surface morphologies were affected by doping. The AFM images in Fig. 4 show that the H<sub>2</sub>SO<sub>4</sub> doped ES membrane has a relatively rough surface with a plating structure while the pristine EB membrane demonstrates a comparatively uniform ridge-and-valley morphology. The roughness parameters (R<sub>a</sub> and R<sub>q</sub>) after the H<sub>2</sub>SO<sub>4</sub> doping process increased from 2.67 nm and 3.36 nm to 5.35 nm and 6.61 nm, respectively.

EB and H<sub>2</sub>SO<sub>4</sub> doped ES membranes display an opposite trend in their charge densities as a function of pH (Fig. 5). This can be explained by the self-doping/dedoping mechanism of the PANI as shown in Scheme 1. At low pH values, the EB membrane has a relatively larger amount of amino and imino-functional groups, hence higher charge density. H<sub>2</sub>SO<sub>4</sub> doping protonates the amine and imine groups, resulting in positively charged nitrogen [45]. On the other hand, negatively charged counter-ion, HSO<sub>4</sub><sup>-</sup>, binds ionically to the positively charged nitrogen [46] resulting in electroneutrality of the polymer backbone. At basic pH values, ES membrane deprotonates due to the removal of H<sub>2</sub>SO<sub>4</sub> from the polymer backbone by OH groups. This

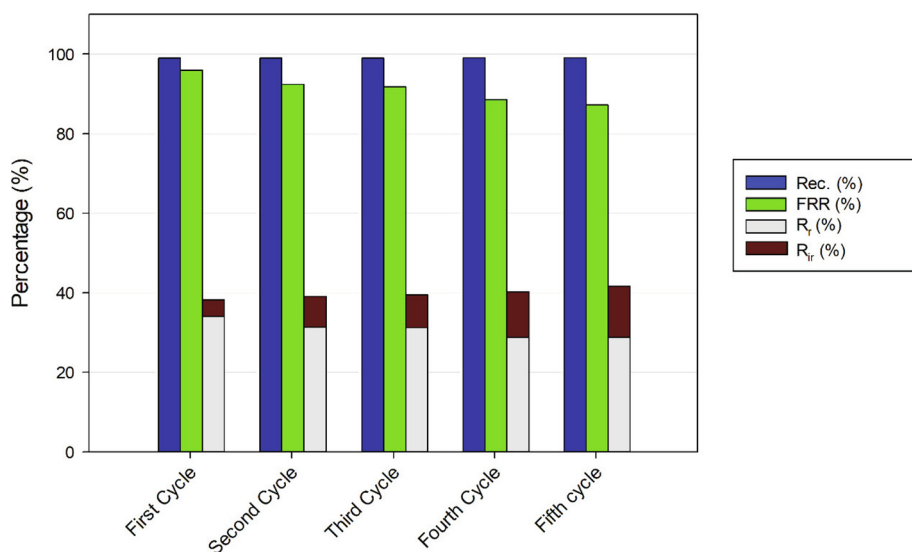
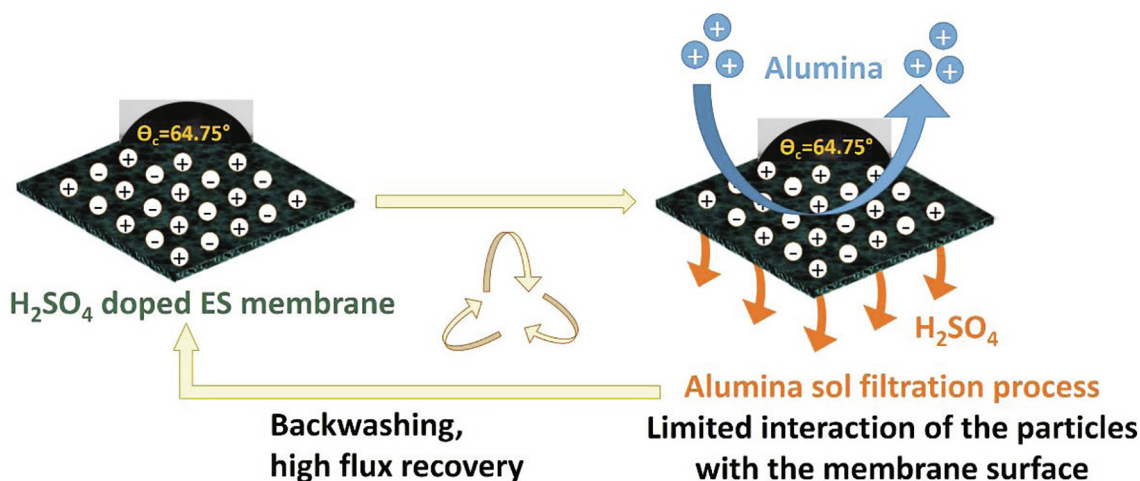


**Fig. 7.** Flux recovery, irreversible and reversible fouling ratios, and alumina sol recoveries for each cycle during filtration of alumina sol.



Scheme 4. Antifouling mechanism of the  $\text{H}_2\text{SO}_4$  doped ES membrane.

resulted in an increase in the positive charge density. EB form of PANI is blue in color while protonation of EB form results in the green ES form [47]. As shown in Fig. 5, the color of the  $\text{H}_2\text{SO}_4$  doped ES membrane changed from green at pH 3 to blue at pH 11 which simply confirmed the dedoping of ES membrane at basic pH. The results in Fig. 5 suggest that the  $\text{H}_2\text{SO}_4$  doped ES membrane is not suitable for treatments in basic environments.

The contact angle value of the EB membrane decreased from  $76.22^\circ \pm 0.85^\circ$  to  $64.75^\circ \pm 2.40^\circ$  upon  $\text{H}_2\text{SO}_4$  doping. The increment of hydrophilicity was due to the hydrophilic sulfonic functional groups of the dopant. Similarly, Liu et al. [48] and Blinova et al. [49] reported an improvement in the hydrophilicity of EB polymer in the presence of doped ions.

Acid doping reduced the *PWP*, *MWCO*, and pore radius of the EB membrane from  $97.57 \pm 1.53 \text{ Lm}^{-2}\text{h}^{-1}\text{bar}^{-1}$ , 7500 Da, and 3.13 nm to  $25.47 \pm 0.06 \text{ Lm}^{-2}\text{h}^{-1}\text{bar}^{-1}$ , 6750 Da, and 2.75 nm, respectively. Slight decreases in the *MWCO* and pore size of the membrane were other evidence of successful acid doping. The acid doping occurred not only on the membrane surface but also in the bulk of the membrane since  $\text{H}_2\text{SO}_4$  can easily penetrate the pores. The decrease in the *PWP* after acid doping can be attributed to pore narrowing within a region near the surface. The proposed mechanism for pore size reduction due to  $\text{H}_2\text{SO}_4$  doping is shown in Scheme 2.

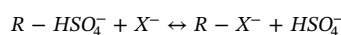
### 3.2. Stability of the $\text{H}_2\text{SO}_4$ doped ES membrane

The stability of the  $\text{H}_2\text{SO}_4$  doped ES membrane was evaluated by comparing the permeability, rejection, surface, bulk morphology, and the chemical structure of the membrane before and after 30 days of  $\text{H}_2\text{SO}_4$  exposure under static conditions. The chemical structures of the fresh and acid-exposed ES membrane were found the same as shown in the ATR-FTIR spectra in Fig. 1.d and .e. Quantitative analysis of SEM-EDX mapping images showed that mass and atomic fractions of O and S elements and their uniform distribution on the surface almost unchanged after acid exposure (Fig. 2.b and .c). In addition, the bulk morphologies of the acid-exposed ES membrane and its fresh counterpart were observed to be similar (Fig. 3.c–.f). Furthermore, no changes were measured in the *PWP* and PEG 6000 rejection of the doped membrane after long-term acid exposure.

Table 1 compares the long-term  $\text{H}_2\text{SO}_4$  stability of membranes prepared from different polymers [15–18,50–53]. Except the poly(2,5-benzimidazole) based membrane (*MWCO*: 6 kDa) which is in the UF category [54], all other membranes tested are in NF range. In the tests, storage time in acid solution ranged from 24 h up to 4 months while the acid concentration was between 0.1 M and 2 M. Exposure to the  $\text{H}_2\text{SO}_4$  concentration higher than 1 M resulted in a significant change in the

permeability and rejection properties of the membranes. When the  $\text{H}_2\text{SO}_4$  concentration was less than 1 M, the doped PANI membrane prepared in our study demonstrated the best performance. Although the commercial NF membrane, MPF-34, was exposed to a significantly lower  $\text{H}_2\text{SO}_4$  concentration than that used in our study, its magnesium and nickel rejections decreased by 27% while *PWP* increased by a factor of 3 [50]. Degradation of the MPF-34 was also shown with SEM and AFM analysis and contact angle measurement.

EB could be easily doped by various organic and inorganic acids. The localized sigma bond in amine groups ( $-\text{NH}_2^+-$ ) along the EB backbone forms a strong chemical bond, while the less strongly localized pi bond in imine groups ( $-\text{NH}^+=$ ) provides a weaker chemical bond [55]. The strengths of the acid and the amine and imine groups in the EB chain determine the ability of the interaction between EB and proton of acid [56]. The acid dissociation constants (*pKa*) for the amine and imine groups in the EB chain were reported as 2.50 and 5.50, respectively [57]. As shown in Scheme 3,  $\text{H}_2\text{SO}_4$  protonates both amine and imine groups in the EB chain since it is a strong acid (*pKa* = 1.92). Protonation equilibria in the  $\text{H}_2\text{SO}_4$  doped ES membrane are influenced by the presence of counterions and change in the pH of the feed solution. When pH becomes higher than the *pKa* of amine and imine groups, the deprotonation of these groups occur and ES membrane returns to EB form. This is a major limitation and restricts the use of  $\text{H}_2\text{SO}_4$  doped ES membrane in a basic pH environment. If the membrane is exposed to a different type of acid solution, the displacement of the anion,  $\text{HSO}_4^-$ , in the polymer backbone ( $\text{R}-\text{HSO}_4^-$ ) with counter anion in solution ( $\text{X}^-$ ) is expected to take place through following ion exchange reaction [58].



The EB membrane was doped with the same acid and at the same pH used in the synthesis of alumina sol. Therefore, the performance of the resulting  $\text{H}_2\text{SO}_4$  doped ES membrane did not change during acidic alumina sol filtration or after 1-month storage in the  $\text{H}_2\text{SO}_4$  solution (Scheme 3).

### 3.3. Alumina sol filtration performance of the $\text{H}_2\text{SO}_4$ doped ES membrane

The  $\text{H}_2\text{SO}_4$  doped ES membrane was used to concentrate alumina sol by filtering the  $\text{H}_2\text{SO}_4$  aqueous solution in sol. Fig. 6 shows the change in flux during 5-cycle sol filtration. The pure water and alumina sol fluxes measured as  $25.47 \pm 0.06 \text{ L/m}^2\text{h}$  and  $15.75 \text{ L/m}^2\text{h}$  at the end of the first cycle decreased to  $22.22 \pm 0.03 \text{ L/m}^2\text{h}$  and  $14.87 \text{ L/m}^2\text{h}$  when 5-cycle filtration was completed. In each cycle, the alumina sol flux decreased rapidly in a short period due to the accumulation of particles on the membrane surface. However, most of the flux was recovered after backwashing the membrane with water for 30 min.

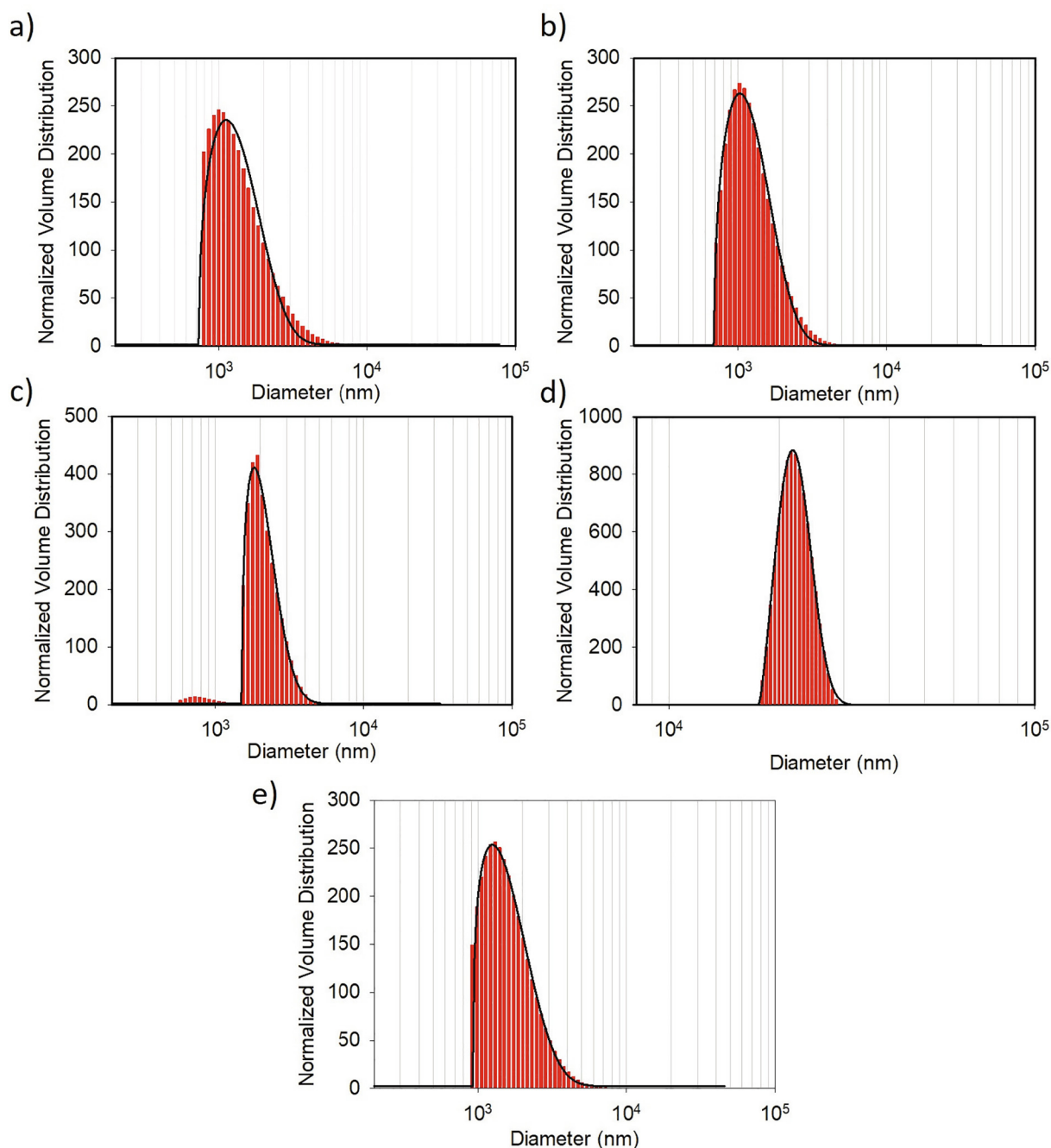


**Fig. 8.** Particle size distributions of a) the prepared alumina sol and powder dried b) at 25 °C after filtering 80% of sol, c) at 25 °C without filtration, d) at 100 °C in an oven without filtration, e) in a freeze dryer without filtration.

Backwashing after 5 h filtration (first cycle) resulted in a 96% flux recovery. The recovery decreased to 87% at the end of the fifth cycle as a result of a gradual increase in irreversible fouling from 4.0% up to 12.70% (Fig. 7). High flux recoveries were observed since the fouling due to accumulation of particles on the surface was mostly reversible.

Fig. 7 demonstrates that 99% of the aluminium sulfate particles were recovered in the retentate stream. The pores on the surface were not clogged by aluminium sulfate particles. This was confirmed by measuring the PEG 6000 rejection at the beginning ( $87.78 \pm 0.38\%$ ) and at the end of 5th filtration cycle ( $89.41 \pm 0.15\%$ ). The results suggest that the  $\text{H}_2\text{SO}_4$  doped ES membrane is a suitable acid-resistant membrane to concentrate alumina sol due to full recovery of particles, high flux restoration achieved after short-time backwashing with DI water and stable rejection performance at the end of 25 h filtration of

extremely acidic alumina sol solution ( $\text{pH} = 0.55$ ).

The antifouling property of the  $\text{H}_2\text{SO}_4$  doped ES membrane can be attributed to the hydrophilicity, surface roughness and net-zero charge of the surface at the filtration pH. The effects of roughness on membrane fouling can vary depending on the interplay between the size of foulant particulates and roughness of the surface [59]. As shown in AFM images (Fig. 4), the ES membrane does not contain large valleys on its surface. The roughness of the membrane is very low compared to the size of the particles and the surface does not have a morphology that can entrap the particles. The hydrophilic charged groups on the polymer backbone create a hydration layer on the surface [60,61], which acts as a physical and energy barrier and prevents the accumulation of the particles. From a thermodynamic point of view, a large amount of energy is needed to break this hydration layer [62]. The

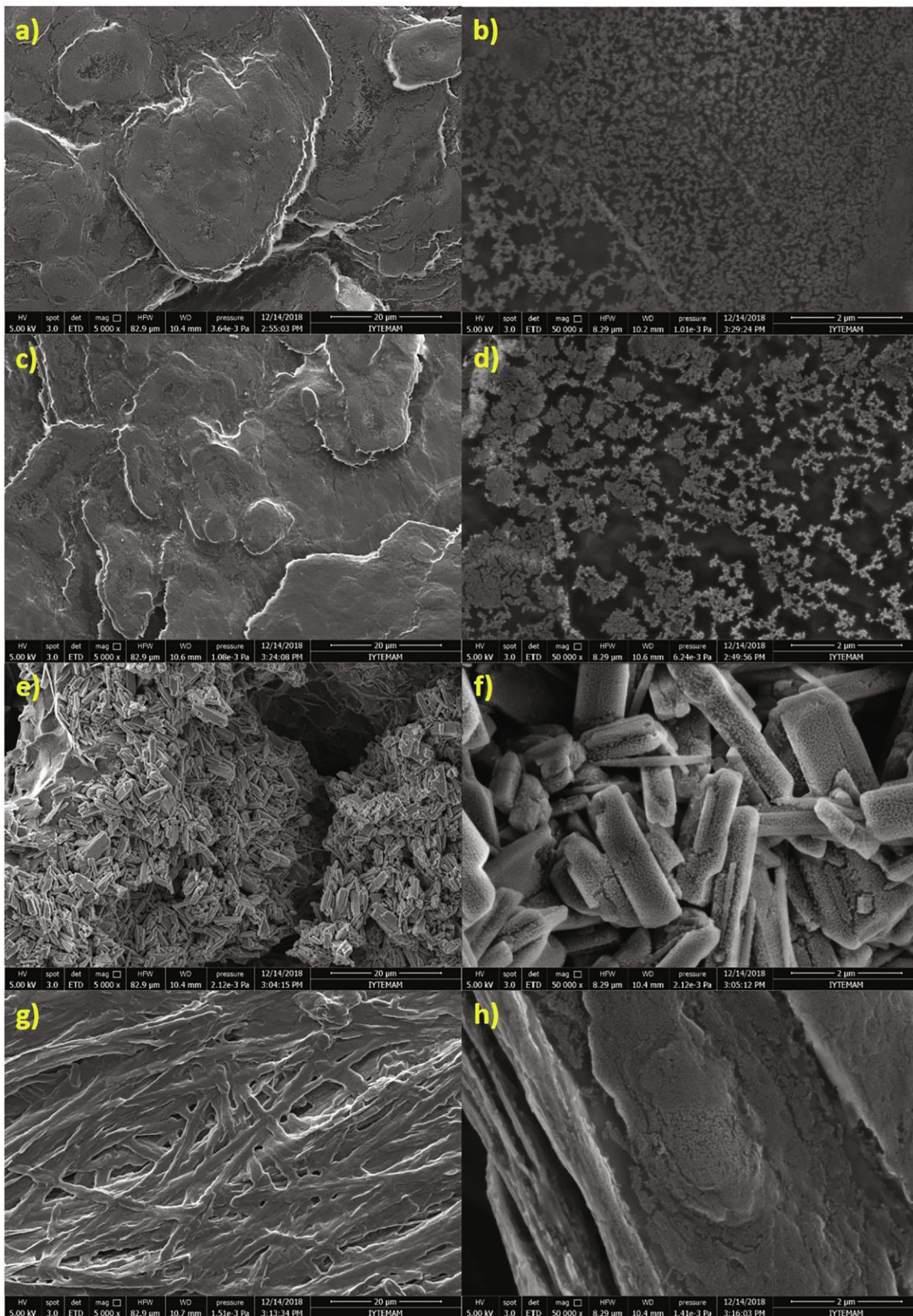


**Fig. 9.** SEM images of the powders dried a-b) at 25 °C after filtering 80% of sol, c-d) at 25 °C without filtration, e-f) at 100 °C in an oven without filtration, g-h) in a freeze dryer without filtration. Magnifications are  $\times 5000$  and  $\times 50000$ , respectively.

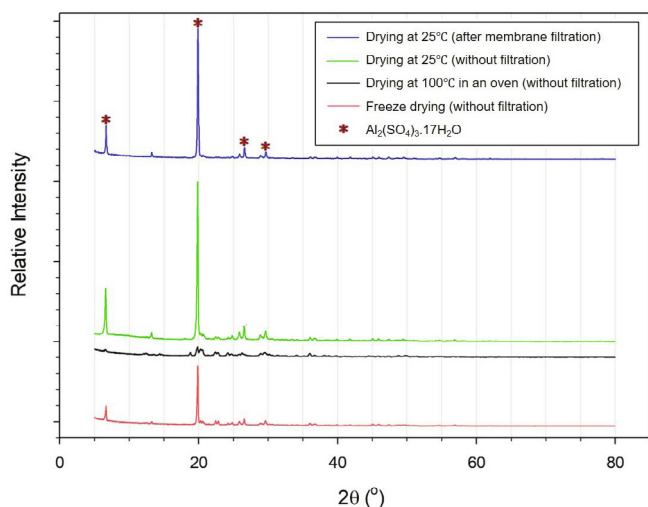


Fig. 10. XRD patterns of the aluminium sulfate powders prepared with membrane filtration and traditional drying methods

Table 2

Comparison of energy cost of powder production with membrane filtration and solely drying-based techniques.

Drying Method	Drying Period	Energy Cost (\$/g)
Drying at 25 °C (after filtering 80% of sol in 25 h)	24 h	0.095
Drying at 25 °C (without filtration)	72 h	–
Freeze-drying (without filtration)	48 h	0.958
Drying at 100 °C in an oven (without filtration)	24 h	0.477

H<sub>2</sub>SO<sub>4</sub> doped ES membrane contains both positively and negatively charged groups (Scheme 4) and has a neutral charge at the filtration pH (Fig. 5). The negatively charged HSO<sub>4</sub><sup>-</sup> and the positively charged nitrogen are closely connected through an ionic bond. This bonding simply avoids interaction of the charged particles with the membrane surface, as shown in Scheme 4. In summary, the antifouling mechanism of the H<sub>2</sub>SO<sub>4</sub> doped ES membrane can be explained by the formation of a hydration layer on the surface and steric hindrance effect of the charged groups, as well as a relatively smooth surface morphology.

### 3.4. The effect of membrane filtration on the chemical and physical properties of the aluminium sulfate powder

To evaluate the influence of membrane filtration on the chemical and physical properties of aluminium sulfate powder, the particle size distribution, morphology and crystalline structures of the powder were determined. After filtering 80% of the H<sub>2</sub>SO<sub>4</sub> solution, the concentrated particles were dried at room temperature without using a dryer.

The mean particle diameter of virgin alumina sol was measured as 1494 ± 201 nm while its polydispersity index (PDI) was 0.495 (Fig. 8). The membrane filtration did not change the size and size distribution of the particles (1211 ± 62 nm, PDI: 0.386). If no filtration was applied, the drying time of the sol at room temperature extended from 24 h to 72 h. Also, larger-sized particles (2102 ± 181 nm with a PDI value of 0.386) were obtained due to their continuous growth during drying of a large volume. For comparison purposes, the powder was also obtained with two additional classical drying techniques without applying filtration, namely, freeze-drying and oven drying at 100 °C. Compared to the membrane filtration usage, the powder produced with freeze-drying had similar size distribution (1760 ± 79 nm, PDI: 0.476) but drying was completed in a longer time (48 h). At 100 °C, the sol was dried in 24 h, however, resulting powder had a

larger size and broad size distribution (22040 ± 2785 nm and PDI: 22.42). Agglomeration of the particles is enhanced at high temperatures due to the combined effects of Van der Waals forces and Brownian motion [30–32].

SEM images of the powder produced by membrane filtration and traditional drying techniques are shown in Fig. 9. The powder obtained with membrane filtration did not include any aggregates and had a fairly smooth appearance (Fig. 9.a and .b). A similar morphology was also observed for the powder dried at room temperature without applying any filtration (Fig. 9.c and .d). Freeze-drying of the sol resulted in a rough structure of fiber layers (Fig. 9.g and .h) while drying in an oven at 100 °C caused interwoven short and stacked fine, needle-like aggregate formation (Fig. 9.e and .f).

XRD patterns shown in Fig. 10 demonstrate that the crystalline structure of the powder dried at room temperature was not deteriorated due to filtration. Except for the powder dried at 100 °C, all the samples contained alunogen (Al<sub>2</sub>(SO<sub>4</sub>)<sub>3</sub>·17H<sub>2</sub>O) which is simple aluminium sulfate, including very high water content. Two intense XRD peaks were observed at 2θ values of ~6.60° and 19.90°, followed by ~26.60° and 29.60°. Freeze-drying reduced the crystallinity of the powder as confirmed by the decrease in the intensity of XRD peaks while oven drying at 100 °C caused even disappearance of the specific XRD peaks at 2θ values of ~26.60° and 29.60°.

Table 2 demonstrates that membrane filtration can significantly reduce the energy cost of powder production (0.095 \$/gram) compared to the cost of traditional drying-based techniques. When operating the filtration unit, energy is needed only in pressurizing the feed using nitrogen. Membrane filtration allows recovering most of the acid and this has also a positive impact both on the cost of production and the environment. The characterization results demonstrated that membrane filtration usage allowed producing aluminium sulfate powder with the most desirable structural features at the lowest energy cost. Filtration of the sol not only reduces drying time but also prevents agglomeration of particles and maintains crystalline structure. These structural properties, in turn, are required for many applications such as the production of high-quality ceramics to obtain uniform particle packing and fully dense materials.

## 4. Conclusion

The self-acid doping ability of PANI is a facile approach to prepare acid-resistant membranes from this polymer. The acid doping procedure proposed in this study is a simple method and can be easily adapted in commercial membrane fabrication processes. The H<sub>2</sub>SO<sub>4</sub> doped PANI membrane preserved its chemical structure and separation performance after 30 days of exposure to the H<sub>2</sub>SO<sub>4</sub> solution under static conditions. In order to obtain long-term acid resistance, the membrane should be doped with the acid in the feed solution and the pH of the dopant should be the same as the pH of feed solution. The H<sub>2</sub>SO<sub>4</sub> doped membrane was successfully used in concentrating the alumina sol synthesized in the H<sub>2</sub>SO<sub>4</sub> solution. Almost 100% of the particles were recovered in the retentate stream and flux loss during filtration was mostly recovered through simple backwashing with water. Concentrating the sol through filtration minimized the risk of uncontrolled particle growth. The concentrated particles were converted into powder form in 24 h simply by drying at room temperature without using a dryer. The features such as long-term acid stability, high particle recovery, low fouling tendency, and low materials and processing costs make acid-doped PANI membrane a potential candidate in the production of aluminium sulfate powder from alumina sol. On the other hand, the membrane can also be used in numerous other applications for the treatment of acid-containing feeds.

## Declaration of Competing Interest

The authors declare that they have no known competing financial

interests or personal relationships that could have appeared to influence the work reported in this paper.

## Acknowledgement

The authors would like to thank Izmir Institute of Technology for the financial support through Grant 2017IYTE43. We also would like to thank the Material Research Centre and Bio-technology and Bioengineering Application Research Centre at the Izmir Institute of Technology for their kind help and technical support.

## References

- J.J. Qin, M.N. Wai, M.H. Do, Integrated ultrafiltration/nanofiltration process for reclamation of wastewater from metal plating industry, *Abstr. Pap. Am. Chem. Soc.* 229 (2005) U924-U924.
- M.J. Gonzalez-Munoz, M.A. Rodriguez, S. Luque, J.R. Alvarez, Recovery of heavy metals from metal industry waste waters by chemical precipitation and nanofiltration, *Desalination* 200 (2006) 742–744, <https://doi.org/10.1016/j.desal.2006.03.498>.
- K. Hayrynen, E. Pongracz, V. Vaisanen, N. Pap, M. Manttari, J. Langwaldt, R.L. Keiski, Concentration of ammonium and nitrate from mine water by reverse osmosis and nanofiltration, *Desalination* 240 (2009) 280–289, <https://doi.org/10.1016/j.desal.2008.02.027>.
- B.C. Ricci, C.D. Ferreira, A.O. Aguiar, M.C.S. Amaral, Integration of nanofiltration and reverse osmosis for metal separation and sulfuric acid recovery from gold mining effluent, *Sep. Purif. Technol.* 154 (2015) 11–21, <https://doi.org/10.1016/j.seppur.2015.08.040>.
- A.G. Boricha, Z.V.P. Murthy, Preparation, characterization and performance of nanofiltration membranes for the treatment of electroplating industry effluent, *Sep. Purif. Technol.* 65 (2009) 282–289, <https://doi.org/10.1016/j.seppur.2008.10.047>.
- M. Manttari, M. Nystrom, Ultrafiltration and nanofiltration in the pulp and paper industry using cross-rotational (CR) filters, *Water Sci. Technol.* 50 (2004) 229–238, <https://doi.org/10.2166/wst.2004.0200>.
- M. Manttari, K. Viitikko, M. Nystrom, Nanofiltration of biologically treated effluents from the pulp and paper industry, *J. Membr. Sci.* 272 (2006) 152–160, <https://doi.org/10.1016/j.memsci.2005.07.031>.
- W. Koschuh, V.H. Thang, S. Krasteva, S. Novalin, K.D. Kulbe, Flux and retention behaviour of nanofiltration and fine ultrafiltration membranes in filtrating juice from a green biorefinery: a membrane screening, *J. Membr. Sci.* 261 (2005) 121–128, <https://doi.org/10.1016/j.memsci.2005.01.049>.
- F. Weinwurm, A. Drljo, A. Friedl, Lignin Concentration by Nanofiltration and precipitation in a lignocellulose biorefinery, in: P.S. Varbanov, J.J. Klemes, S.R.W. Alwi, J.Y. Yong, X. Liu (Eds.) *Pres15: Process Integration, Modelling and Optimisation for Energy Saving and Pollution Reduction*, Aidic Servizi Srl, Milano, 2015, pp. 901–906.
- T.R. Gaboriski, J.L. Snyder, C.C. Striemer, D.Z. Fang, M. Hoffman, P.M. Fauchet, J.L. McGrath, High-performance separation of nanoparticles with ultrathin porous nanocrystalline silicon membranes, *ACS Nano* 4 (2010) 6973–6981, <https://doi.org/10.1021/nn102064c>.
- T.K. Mudalige, H. Qu, G. Sánchez-Pomales, P.N. Sisco, S.W. Linder, Simple functionalization strategies for enhancing nanoparticle separation and recovery with asymmetric flow field flow fractionation, *Anal. Chem.* 87 (2015) 1764–1772, <https://doi.org/10.1021/ac.503683n>.
- B. Meisterjahn, S. Wagner, F. von der Kammer, D. Hennecke, T. Hofmann, Silver and gold nanoparticle separation using asymmetrical flow-field flow fractionation: Influence of run conditions and of particle and membrane charges, *J. Chromatogr. A* 1440 (2016) 150–159, <https://doi.org/10.1016/j.chroma.2016.02.059>.
- N. Alele, R. Streubel, L. Gamrad, S. Barcikowski, M. Ulbricht, Ultrafiltration membrane-based purification of bioconjugated gold nanoparticle dispersions, *Sep. Purif. Technol.* 157 (2016) 120–130, <https://doi.org/10.1016/j.seppur.2015.11.033>.
- C. Van Goethem, M. Mertens, F.G. Cirujano, J.W. Seo, D. De Vos, I.F.J. Vankelecom, Improved MOF nanoparticle recovery and purification using crosslinked PVDF membranes, *Chem. Commun.* 54 (2018) 7370–7373, <https://doi.org/10.1039/C8CC04326D>.
- M. Liu, G. Yao, Q. Cheng, M. Ma, S. Yu, C. Gao, Acid stable thin-film composite membrane for nanofiltration prepared from naphthalene-1,3,6-trisulfonfylchloride (NTSC) and piperazine (PIP), *J. Membr. Sci.* 415–416 (2012) 122–131, <https://doi.org/10.1016/j.memsci.2012.04.043>.
- Y. Zeng, L. Wang, L. Zhang, J.Q. Yu, An acid resistant nanofiltration membrane prepared from a precursor of poly(s-triazine-amine) by interfacial polymerization, *J. Membr. Sci.* 546 (2018) 225–233, <https://doi.org/10.1016/j.memsci.2017.10.022>.
- M. He, T. Yuan, W. Dong, P. Li, Q. Jason Niu, J. Meng, High-performance acid-stable polysulfonamide thin-film composite membrane prepared via spinning-assist multilayer interfacial polymerization, *J. Mater. Sci.* 54 (2019) 886–900, <https://doi.org/10.1007/s10853-018-2847-6>.
- H. Hoseinpour, M. Peyravi, A. Nozad, M. Jahanshahi, Static and dynamic assessments of polysulfonamide and poly(amide-sulfonamide) acid-stable membranes, *J. Taiwan. Inst. Chem. Eng.* 67 (2016) 453–466, <https://doi.org/10.1016/j.jtice.2016.07.039>.
- T. Yeerken, G. Wang, H. Li, H.L. Liu, W.D. Yu, Chemical stable, superhydrophobic and self-cleaning fabrics prepared by two-step coating of a polytetrafluoroethylene membrane and silica nanoparticles, *Text. Res. J.* 89 (2019) 4827–4841, <https://doi.org/10.1177/0040517519842795>.
- W. Zhang, Z. Shi, F. Zhang, X. Liu, J. Jin, L. Jiang, Superhydrophobic and superoleophilic PVDF membranes for effective separation of water-in-oil emulsions with high flux, *Adv. Mater.* 25 (2013) 2071–2076, <https://doi.org/10.1002/adma.201204520>.
- C. Peng, S. Xing, Z. Yuan, J. Xiao, C. Wang, J. Zeng, Preparation and anti-icing of superhydrophobic PVDF coating on a wind turbine blade, *Appl. Surf. Sci.* 259 (2012) 764–768, <https://doi.org/10.1016/j.apsusc.2012.07.118>.
- S.-H. Park, S.J. Kwon, M.G. Shin, M.S. Park, J.S. Lee, C.H. Park, H. Park, J.-H. Lee, Polyethylene-supported high performance reverse osmosis membranes with enhanced mechanical and chemical durability, *Desalination* 436 (2018) 28–38, <https://doi.org/10.1016/j.desal.2018.02.007>.
- J. da Silva Bursal, L.G. Peeva, S. Kumbharkar, A. Livingston, Organic solvent resistant poly(ether-ether-ketone) nanofiltration membranes, *J. Membr. Sci.* 479 (2015) 105–116, <https://doi.org/10.1016/j.memsci.2014.12.035>.
- L.W. McKeen, 1 - Fluoropolymers, in: L.W. McKeen (Ed.) *Fluorinated Coatings and Finishes Handbook* (Sec. Ed.), William Andrew Publishing, Oxford, 2016, pp. 1–12.
- S. Ebnesaajad, 13 - Properties of Fluoropolymers, in: S. Ebnesaajad (Ed.) *Melt Processible Fluoroplastics*, William Andrew Publishing, Norwich, NY, 2003, pp. 375–447.
- J. Shen, S. Shahid, A. Sarihan, D.A. Patterson, E.A.C. Emanuelsson, Effect of polyacid dopants on the performance of polyaniline membranes in organic solvent nanofiltration, *Sep. Purif. Technol.* 204 (2018) 336–344, <https://doi.org/10.1016/j.seppur.2018.04.034>.
- Z.A. Boeva, V.G.J. Sergeyev, Polyaniline: synthesis, properties, and application, *Polyaniline: synthesis, properties, and application*, *Polym Sci Ser C* 56 (2014) 144–153, <https://doi.org/10.1134/S1811238214010032>.
- E. Ponthieu, E. Payen, G.M. Pajonk, J. Grimblot, Comparison of drying procedures for the preparation of alumina powders with the system Al-alkoxide/tertiary butanol/water, *J. Sol-Gel Sci. Technol.* 8 (1997) 201–206, <https://doi.org/10.1007/BF02436841>.
- H.K. Varma, T.V. Mani, A.D. Damodaran, K.G. Warriar, U. Balachandran, Characteristics of alumina powders prepared by spray-drying of boehmite sol, *J. Am. Ceram. Soc.* 77 (1994) 1597–1600, <https://doi.org/10.1111/j.1151-2916.1994.tb09762.x>.
- S. Kwon, G.L. Messing, The effect of particle solubility on the strength of nanocrystalline agglomerates: Boehmite, *Nanostruct. Mater.* 8 (1997) 399–418, [https://doi.org/10.1016/S0965-9773\(97\)00180-3](https://doi.org/10.1016/S0965-9773(97)00180-3).
- I.A. Rahman, P. Vejayakumaran, C.S. Sipaut, J. Ismail, C.K. Chee, Effect of the drying techniques on the morphology of silica nanoparticles synthesized via sol-gel process, *Ceram. Int.* 34 (2008) 2059–2066, <https://doi.org/10.1016/j.ceramint.2007.08.014>.
- R.G. Frey, J.W. Halloran, Compaction behavior of spray-dried alumina, *J. Am. Ceram. Soc.* 67 (1984) 199–203, <https://doi.org/10.1111/j.1151-2916.1984.tb19742.x>.
- E.C. Gomes, M.A.S. Oliveira, Chemical polymerization of aniline in hydrochloric acid (HCl) and formic acid (HCOOH) media. Differences between the two synthesized polyanilines, *Am. J. Polym. Sci.* 2 (2012) 5–13, <https://doi.org/10.5923/j.ajps.20120202.02>.
- K.A. Ibrahim, Synthesis and characterization of polyaniline and poly(aniline-co-oxynitroaniline) using vibrational spectroscopy, *Arab. J. Chem.* 10 (2017) S2668–S2674. DOI: 10.1016/j.arabj.2013.10.010.
- J. Luo, L. Ding, Y. Su, S. Wei, Y. Wan, Concentration polarization in concentrated saline solution during desalination of iron dextran by nanofiltration, *J. Membr. Sci.* 363 (2010) 170–179, <https://doi.org/10.1016/j.memsci.2010.07.033>.
- C. Combe, E. Molis, P. Lucas, R. Riley, M.M. Clark, The effect of CA membrane properties on adsorptive fouling by humic acid, *J. Membr. Sci.* 154 (1999) 73–87, [https://doi.org/10.1016/S0376-7388\(98\)00268-3](https://doi.org/10.1016/S0376-7388(98)00268-3).
- W. Richard Bowen, T.A. Doneva, Atomic force microscopy characterization of ultrafiltration membranes: Correspondence between surface pore dimensions and molecular weight cut-off, *Surf. Interface Anal.* 29 (2000) 544–547, [https://doi.org/10.1002/1096-9918\(200008\)29:8<544::AID-SIA901>3.0.CO;2-4](https://doi.org/10.1002/1096-9918(200008)29:8<544::AID-SIA901>3.0.CO;2-4).
- B.E. Yoldas, Alumina gels that form porous transparent Al<sub>2</sub>O<sub>3</sub>, *J. Mater. Sci.* 10 (1975) 1856–1860, <https://doi.org/10.1007/BF00754473>.
- JCPDS-ICDD, PDF-2 Database, International Centre for Diffraction Data, Pennsylvania (2000).
- G. Dognani, P. Hadi, H. Ma, F.C. Cabrera, A.E. Job, D.L.S. Agostini, B.S. Hsiao, Effective chromium removal from water by polyaniline-coated electrospun adsorbent membrane, *Chem. Eng. J.* 372 (2019) 341–351, <https://doi.org/10.1016/j.cej.2019.04.154>.
- S. Wang, F. Liu, C. Gao, T. Wan, L. Wang, L. Wang, L. Wang, Enhancement of the thermoelectric property of nanostructured polyaniline/carbon nanotube composites by introducing pyrrole unit onto polyaniline backbone via a sustainable method, *Chem. Eng. J.* 370 (2019) 322–329, <https://doi.org/10.1016/j.cej.2019.03.155>.
- M. Trchová, I. Šeděnková, E. Tobolková, J. Stejskal, FTIR spectroscopic and conductivity study of the thermal degradation of polyaniline films, *Polym. Degrad. Stab.* 86 (2004) 179–185, <https://doi.org/10.1016/j.polymdegradstab.2004.04.011>.
- X. Huang, B.T. McVerry, C. Marambio-Jones, M.C.Y. Wong, E.M.V. Hoek, R.B. Kaner, Novel chlorine resistant low-fouling ultrafiltration membrane based on a hydrophilic polyaniline derivative, *J. Mater. Chem. A* 3 (2015) 8725–8733, <https://doi.org/10.1039/C5TA00900F>.
- N.V. Blinova, J. Stejskal, M. Trchová, J. Prokeš, M. Omastová, Polyaniline and

- polypyrrole: a comparative study of the preparation, *Eur. Polym. J.* 43 (2007) 2331–2341, <https://doi.org/10.1016/j.eurpolymj.2007.03.045>.
- [45] E.T. Kang, K.G. Neoh, K.L. Tan, Polyaniline: a polymer with many interesting intrinsic redox states, *Prog. Polym. Sci.* 23 (1998) 277–324, [https://doi.org/10.1016/S0079-6700\(97\)00030-0](https://doi.org/10.1016/S0079-6700(97)00030-0).
- [46] E.T. Kang, K.G. Neoh, S.H. Khor, K.L. Tan, B.T.G. Tan, X.p.s. studies of charge transfer interactions in some polyaniline complexes, *Polym.* 31 (1990) 202–207, [https://doi.org/10.1016/0032-3861\(90\)90106-9](https://doi.org/10.1016/0032-3861(90)90106-9).
- [47] T. Ogoshi, Y. Hasegawa, T. Aoki, Y. Ishimori, S. Inagi, T. Yamagishi, Reduction of emeraldine base form of polyaniline by Pillar[5]arene based on formation of poly (pseudorotaxane) structure, *Macromolecules* 44 (2011) 7639–7644, <https://doi.org/10.1021/ma2016979>.
- [48] M.J. Liu, K. Tzou, R.V. Gregory, Influence of the doping conditions on the surface energies of conducting polymers, *Synth. Met.* 63 (1994) 67–71, [https://doi.org/10.1016/0379-6779\(94\)90251-8](https://doi.org/10.1016/0379-6779(94)90251-8).
- [49] N.V. Blinova, J. Stejskal, M. Trchová, J. Prokeš, Control of polyaniline conductivity and contact angles by partial protonation, *Polym. Int.* 57 (2008) 66–69, <https://doi.org/10.1002/pi.2312>.
- [50] B.C. Ricci, C.D. Ferreira, L.S. Marques, S.S. Martins, B.G. Reis, M.C.S. Amaral, Assessment of the chemical stability of nanofiltration and reverse osmosis membranes employed in treatment of acid gold mining effluent, *Sep. Purif. Technol.* 174 (2017) 301–311, <https://doi.org/10.1016/j.seppur.2016.11.007>.
- [51] S. Platt, M. Nyström, A. Bottino, G. Capannelli, Stability of NF membranes under extreme acidic conditions, *J. Membr. Sci.* 239 (2004) 91–103, <https://doi.org/10.1016/j.memsci.2003.09.030>.
- [52] H. Wang, Z. Wei, H. Wang, H. Jiang, Y. Li, C. Wu, An acid-stable positively charged polysulfonamide nanofiltration membrane prepared by interfacial polymerization of polyallylamine and 1,3-benzenedisulfonyl chloride for water treatment, *RSC Adv.* 9 (2019) 2042–2054, <https://doi.org/10.1039/C8RA08369J>.
- [53] Y. Zhu, P. Dou, H. He, H. Lan, S. Xu, Y. Zhang, T. He, J. Niu, Improvement of permeability and rejection of an acid resistant polysulfonamide thin-film composite nanofiltration membrane by a sulfonated poly(ether ether ketone) interlayer, *Sep. Purif. Technol.* 239 (2020) 116528, <https://doi.org/10.1016/j.seppur.2020.116528>.
- [54] H.R. Lohokare, H.D. Chaudhari, U.K. Kharul, Solvent and pH-stable poly(2,5-benzimidazole) (ABPBI) based UF membranes: preparation and characterizations, *J. Membr. Sci.* 563 (2018) 743–751, <https://doi.org/10.1016/j.memsci.2018.06.052>.
- [55] G. Rimbui, I. Stamatin, C.L. Jackson, K. Scott, The morphology control of polyaniline as conducting polymer in fuel cell technology, *J. Optoelectron. Adv. Mater.* 8 (2006) 670–674.
- [56] D.W. Hatchett, M. Josowicz, J. Janata, Acid doping of polyaniline: Spectroscopic and electrochemical studies, *J. Phys. Chem. B* 103 (1999) 10992–10998, <https://doi.org/10.1021/jp991110z>.
- [57] C. Menardo, M. Nechtschein, A. Rousseau, J.P. Travers, P. Hany, Investigation on the structure of polyaniline: 13C n.m.r. and titration studies, *Synth. Met.* 25 (1988) 311–322, [https://doi.org/10.1016/0379-6779\(88\)90571-1](https://doi.org/10.1016/0379-6779(88)90571-1).
- [58] N. Endo, Y. Takeda, K. Matsusaki, M. Higa, Separation and concentration of trace ion with polyaniline, *Anal. Sci.* 17 (2001), <https://doi.org/10.14891/analscisp.17icas.0.11109.0>.
- [59] L. Bai, H. Wu, J. Ding, A. Ding, X. Zhang, N. Ren, G. Li, H. Liang, Cellulose nanocrystal-blended polyethersulfone membranes for enhanced removal of natural organic matter and alleviation of membrane fouling, *Chem. Eng. J.* 382 (2020) 122919, <https://doi.org/10.1016/j.cej.2019.122919>.
- [60] C. Liu, Y. Liu, Y. Guo, C. Wang, Z. Hu, C. Zhang, High-hydrophilic and salt rejecting PA-g/co-PVP RO membrane via bionic sand-fixing grass for pharmaceutical wastewater treatment, *Chem. Eng. J.* 357 (2019) 269–279, <https://doi.org/10.1016/j.cej.2018.09.151>.
- [61] Z. Zhu, J. Jiang, X. Wang, X. Huo, Y. Xu, Q. Li, L. Wang, Improving the hydrophilic and antifouling properties of polyvinylidene fluoride membrane by incorporation of novel nanohybrid GO@SiO<sub>2</sub> particles, *Chem. Eng. J.* 314 (2017) 266–276, <https://doi.org/10.1016/j.cej.2016.12.038>.
- [62] M. He, K. Gao, L. Zhou, Z. Jiao, M. Wu, J. Cao, X. You, Z. Cai, Y. Su, Z. Jiang, Zwitterionic materials for antifouling membrane surface construction, *Acta Biomater.* 40 (2016) 142–152, <https://doi.org/10.1016/j.actbio.2016.03.038>.